Physics – Uspekhi **40** (9) 963 – 974 (1997)

CONFERENCES AND SYMPOSIA PACS number: 01.10.Fv

Scientific session of the Division of General Physics and Astronomy of the Russian Academy of Sciences (23 April 1997)

A scientific session of the Division of General Physics and Astronomy of the Russian Academy of Sciences was held on 23 April 1997 at the P L Kapitza Institute for Physical Problems. The following reports were presented at the session:

(1) **Simonov V I** (Institute of Crystallography, RAS, Moscow) "Structural investigation of single crystals and the structure – properties correlation";

(2) **Fridman A M** (Institute for Astronomy, RAS, Moscow) "Giant curls in galaxies";

(3) **Balaev A D, Val'kov V V, Gavrichkov V A, Ivanova N B, Ovchinnikov S G, Chernov V K** (Kirenskiĭ Institute of Physics, RAS, Krasnoyarsk) "Quantum oscillations of resistance and magnetization in magnetic semiconductors and semimetals";

(4) **Brazhkin V V, Lyapin A G, Popova S V, Voloshin R N** (Institute of High Pressure Physics, RAS, Troitsk, Moscow Region), **Lyapin S G** (Institute of High Pressure Physics and University of Oxford, Clarendon Laboratory, Oxford), **Klyuev Yu A, Naletov A M** (All-Russia Scientific-Research Institute of Diamonds), **Mel'nik N N** (P N Lebedev Physics Institute, RAS, Moscow) "New crystalline and amorphous carbon modifications produced from fullerite at high pressure";

(5) **Ragul'skiĭ V V** (Institute for Mechanical Problems, RAS, Moscow) "An experimental study of the optical isotropy of space";

(6) **Kravtsov A V, Komberg B V, Lukash V N** (Astro-Space Centre of the P N Lebedev Physics Institute, RAS, Moscow) "Large-scale structure of the Universe and quasars".

Summaries of the four (1, 3, 4, 5) reports are given below.

PACS numbers: 61.66.Fn, **61.90.+d**

Structural investigation of single crystals and the structure – properties correlation

V I Simonov

The diffraction of X-rays, electrons or neutrons in crystals allows information to be obtained on the atomic, real (imperfect) and electronic structure of crystalline materials. Especially informative are structural studies of single crystals which make it possible not only to fix the atomic positions in a crystal with an accuracy of a few milliangstroms, but also to determine reliably the parameters of thermal atomic motion, with regard to anisotropy and anharmonism, as well as the character of interatomic bonds in the compound under analysis. The central problem of structural analysis is to establish regular relationships between the structure and properties of crystalline materials. Knowledge of these correlations opens up ways for the deliberate search and synthesis of new crystals and modification of well-known materials by means of isomorphous atomic replacements. The latter involves the possibility of regulating the physical properties of crystals within certain limits. A successful solution to the problem of producing new crystalline materials with properties interesting to both solid state physics and practical materials science depends on the collaboration of different-profile specialists. It is necessary to join the efforts of those engaged in the investigation of the growth, structure and properties of crystalline materials.

The most efficient way to establish the structure – properties correlations in crystals is to study at the atomic level phase transitions in solids. Comparison of the structural changes occurring in the course of a first-order phase transition with the crystal properties before and after the transition provides a direct answer to whether the physical properties of a crystal are due to one or another feature of its structure. Until recently, structural analysis has been regarded as practically useless for studying second-order phase transitions, when the atomic positions in the structure remain unchanged to a first approximation. Not long ago, a structural investigation of the superconducting transition in a single crystal of one of the high-temperature superconductors [1] established anomalies in the behaviour of thermal atomic vibrations in the neighbourhood of the phase transition, depending on the temperature. Atomic thermal motion in a crystal is determined by the geometry and chemical bond character of a given atom in the structure. Chemical bonds are, in turn, a derivative of the electronic structure of a crystal. Thus, the change of electronic structure of a crystal in the process of a second-order phase transition can be judged from investigations of the behaviour of thermal atomic motion in the vicinity of the transition.

Below, inorganic compounds of different types are used to illustrate the results of precise structural investigations of corresponding single crystals and the establishment of structure – properties correlations.

Fluorite-type nonstoichiometric phases

The mineral fluorite, CaF_2, invariably contains an isomorphic impurity of rare earth elements. On the basis of fluorite's structural type, a great number of solid solutions have been synthesized with the composition $M^{2+}_{1-x}R^{3+}_{x}F_{2+x}$, where $M \equiv$ Ca, Sr, Ba and other bivalent cations, whereas R represents the entire series of rare earth elements from lanthanum to lutetium, and yttrium. Interest in the crystals of such compounds is due to their physical properties: they

Uspekhi Fizicheskikh Nauk **167** (9) 1013 – 1024 (1997)
Translated by M V Magnitskaya, K A Postnov; edited by A Radzig

find a wide use as infrared optics elements, serve as matrices for developing lasers, are superionic conductors with high fluoride ion conductivity and, as acoustic materials, allow the ultrasonic velocity to be changed in a controllable way, depending on the composition. Figure 1a presents the composition dependences of ionic conductivity for two compound series, $Ba_{0.9}R_{0.1}F_{2.1}$ and $Ca_{0.9}R_{0.1}F_{2.1}$, where R represents different rare earth elements. The reason for the dissimilar dependences in these crystal series may be understood only on the basis of the atomic structure analysis of the corresponding solid solutions. As has been demonstrated by structural investigations, rare earth elements in such compounds are not uniformly distributed to substitute bivalent cations. Clusters always form in the structure of a solid solution [2]. As this takes place, some F atoms leave their sites, and the resultant cavities accommodate the atoms of rare earth elements and the F atoms to compensate those escaping from their regular sites and the excess valency of rare earth cations. As was shown in Ref. [3], clusters of different structure form, depending on the ionic radii ratio for the M^{2+} and R^{3+} cations. For BaF_2-based compounds with any rare earth element, the clusters have the same structure. In the case of a CaF_2 matrix with rare earth cations of either half of the series, clusters of two essentially different kinds form (Fig. 1b). This is the reason for the dissimilar conductivity dependences on composition presented in Fig. 1a. The ionic conductivity – structure correlation being established, one is able, by varying the composition of solid solutions, to grow crystals, whose conductivity may be deliberately and smoothly changed from crystal to crystal over 4 – 5 orders of magnitude. The ranges for other physical properties in such crystals are not so wide. So, single crystals of BaF_2 and $Ba_{0.69}La_{0.31}F_{2.31}$ are characterized by {111} face hardness equal to 80 and 250 kg mm^{-2}, respectively. By changing the lanthanum content, one may obtain a crystal with any value of hardness within the range specified. Similarly, the melting temperature, the refraction coefficients for infrared light, the cubic unit cell parameters, etc., are susceptible to variations.

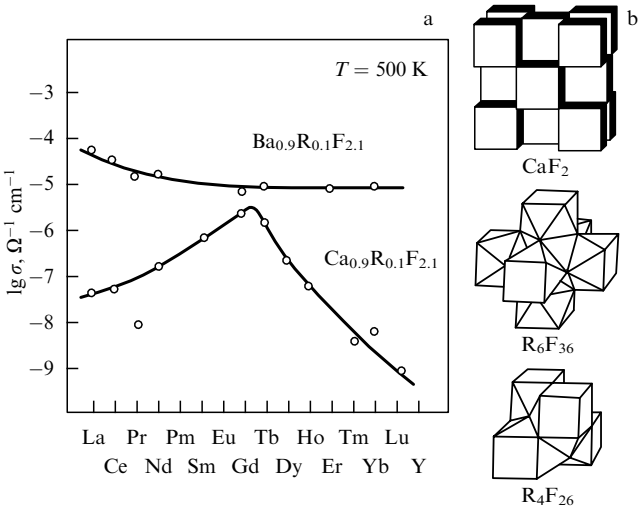

Figure 1. (a) Composition dependence of F^{1-} ion electroconductivity in two series of solid solutions, $Ba_{0.9}R_{0.1}F_{2.1}$ and $Ca_{0.9}R_{0.1}F_{2.1}$. (b) The structure of CaF_2 fluorite (with Ca in the centres and F in the vertices of occupied cubes); R_6F_{36} clusters which are formed in all BaF_2-based solid solutions and in CaF_2-based solid solutions with elements of the second half of rare earth series, and R_4F_{26} clusters which characterize CaF_2-based solid solutions with elements of the first half of the rare earth series.

Sillenites

To date, over 50 compounds with the structural type of $Bi_{12}MO_{20}$ sillenite have been synthesized, in which the role of M cations is played by Si, Ge, Ti, (Ga, P), (Bi, Zn), etc. The absence of the inversion centre in sillenites, in comparison with fluorites, permits the physical properties characterized by odd-rank tensors. It is the rich variety of physical properties that arouses interest in sillenites. The piezoelectric, electro-optic and photoconducting properties make sillenites popular in piezotechnology, acousto- and optoelectronics. The low velocity of propagation of ultrasound and the high value of the piezoelectric modulus are responsible for their successful application in delay lines, resonators, and surface wave amplifiers. High photosensitivity combined with the electrooptic effect enables sillenites to be employed in space-time light modulators and for recording phase holograms. In fact, only $Bi_{12}SiO_{20}$ and $Bi_{12}GeO_{20}$ sillenites have found practical uses so far. Neutron-diffraction investigations of the structure of sillenite solid solutions, when different isomorphic mixtures of atoms play the part of M cations, show that the potentials for deliberately modifying the physical properties of sillenite have hardly begun. The structural analysis of single sillenite crystals, with the M crystallographic position being occupied by Ti, (Fe, P), (Bi, Ga), (Bi, Fe), (Bi, Zn) or (Bi, V) [4], has revealed a rich variety of atomic mechanisms for isomorphic substitutions in the corresponding solid solutions. Whereas only two types of clusters in fluorites provide a great scope for modifying their properties, the opportunities in sillenites are far more abundant. Figure 2a presents the stoichiometric sillenite structure realized when Si or Ge atoms play the role of M cations. Further, Figs 2b – e display fragments of structures, with the M site occupied by Ti, (Fe, P), (Bi, Ga), (Bi, Fe), (Bi, Zn) and (Bi, V) cations. Sillenites were previously [5] assumed to be invariably stoichiometric, strictly corresponding to the formula $Bi_{12}MO_{20}$, with the effective valency of M cation being four, even in solid solutions. In this case, there are always 20 oxygens per formula unit. A study reported in Ref. [4] shows this is true only for $M \equiv Si$ or Ge. With $M \equiv Ti$, a titanium-and-oxygen defective $Bi_{12}Ti_{0.90}O_{19.80}$ structure arises (Fig. 2b). The cation vacancies are established in compound $Bi_{12}(Fe^{3+}_{0.35}P^{5+}_{0.59})O_{20}$, too (Fig. 2c). The mechanism of isomorphic substitutions in compounds is more complicated when the M positions are partially occupied by the Bi cations. Bismuth was believed [5] to have a valency of five (Bi^{5+}), because the Bi^{3+} ion is too large to be accommodated within the M tetrahedron. It was, however, proved [4] that in bismuth compounds, not an individual cation, but the $[MO_4]$ tetrahedron is substituted by the umbrella-shaped $[Bi^{3+}O_3]$ group in the M position, with a non-shared electron pair of the Bi^{3+} cation occuring on the site lacking oxygen (Fig. 2d). As this takes place, the compounds $Bi_{12}(Bi_{0.50}Ga_{0.50})O_{19.50}$, $Bi_{12}(Bi_{0.50}Fe_{0.50})O_{19.50}$ and $Bi_{12}(Bi_{0.67}Zn_{0.33})O_{19.33}$ form. The statistical orientation of the umbrella-shaped group keeps the crystal symmetry cubic, but now only on average. Clusters of even more complex character form in the compound $Bi_{12}(Bi_{0.03}V_{0.89})O_{20.27}$ (Fig. 2e). To compensate the charge of five-valent vanadium, over 20 O atoms per formula unit appear in the structure. The excess oxygens are accommodated within the structure cavities and reliably located by means of neutron diffraction. There is no doubt that the structural study of sillenites of different composition will reveal other mechanisms of isomorphic substitution. The

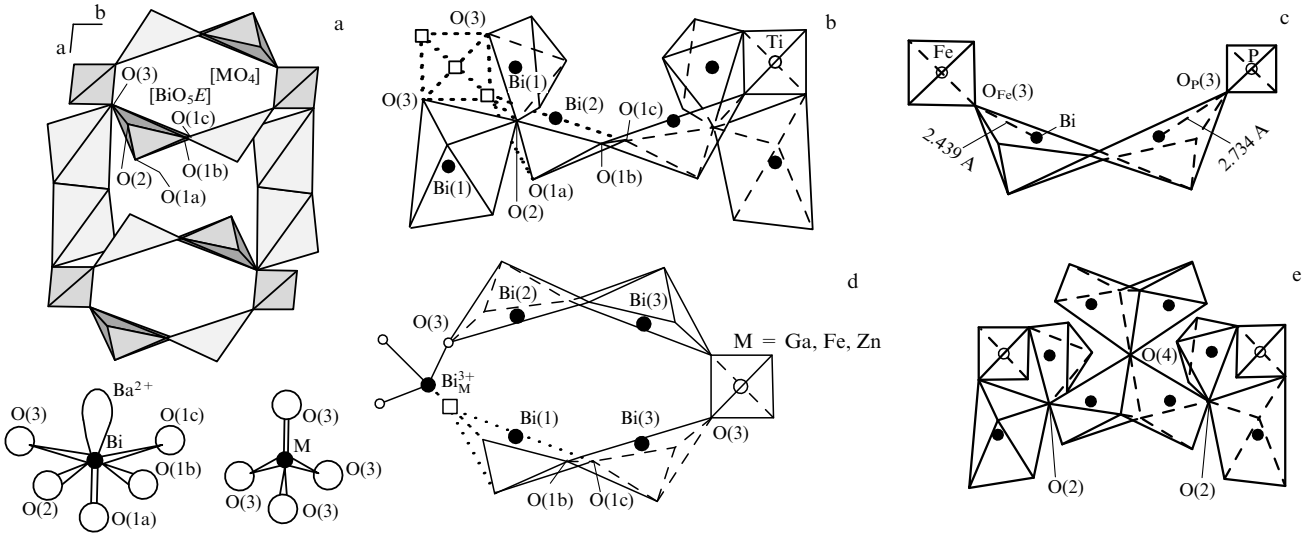

Figure 2. Structure of stoichiometric sillenite $Bi_{12}MO_{20}$, and the structures of $[BiO_5]$ polyhedrons and $[MO_4]$ tetrahedrons (a). Fragments of sillenite structures with different atoms on the M crystallographic site: Ti (b); (Fe, P) (c); (Bi, Ga), (Bi, Fe) or (Bi, Zn) (d); (Bi, V) (e).

broad spectrum of structure variations in sillenites leads to a rich variety of physical properties. There are strong grounds to believe that sillenites will be high on the list of crystals with peculiar physical properties.

Structural changes at the second-order phase transition

Precise structural investigations of phase transitions to the superconducting state in high-temperature superconductors provide additional information on the mechanism of such transitions. As noted above, for structural analysis of single crystals in the neighbourhood of a second-order phase transition, special attention is paid to the behaviour of thermal atomic vibrations. However, to obtain reliable values of the thermal vibration parameters, one needs with high accuracy to fix the atomic coordinates, the scheme of isomorphic substitutions, the disordering in the arrangement of atoms, if available, and other structural parameters. Precise structural investigations have established that the transition to the superconducting state in a crystal is pronounced in the behaviour of interatomic distances in the structure. For example, Figure 3 for the structure of $YBa_2Cu_4O_8$, $T_c = 72$ K, represents the behaviour of Cu1–O1 and Cu2–O1 interatomic distances, where Cu1 and Cu2 atoms are from the double band and from the cuprate plane of the structure, respectively. Oxygen O1 enters the Cu1-atom quadratic coordination and is apical for the cuprate-plane copper Cu2. The behaviour of distances suggests the redistribution of valence forces in favour of the Cu2–O1 bond in the process of the superconducting transition.

The anomalous behaviour of thermal atomic vibrations at the superconducting transition of a single-crystal $Tl_2Ba_2CaCu_2O_8$, $T_c = 110$ K, is shown in Fig. 4. The change of thermal vibrations over the phase transition is most characteristic of the O1 atom from the cuprate network of the structure. Each of these atoms is involved in the strong bonds –Cu–O1–Cu–. The figure presents the behaviour of the principal axes of the general ellipsoid of the O1 atom thermal vibrations: the minimum vibration amplitude is along the strong bond Cu–O, the maximum is in the direction perpendicular to the cuprate plane (Fig. 4a). For comparison, Fig. 4b presents the behaviour of Ca-atom thermal vibrations, which are characterized by the ellipsoid of revolution extended along the crystal *c*-axis [1].

Precise structural data are of significance not only in the search for new materials and the modification of well-known ones. They are of principal importance in passing from the phenomenological description of the properties and phenomena that occur in crystals under external influences to the microscopic theory of these properties and phenomena.

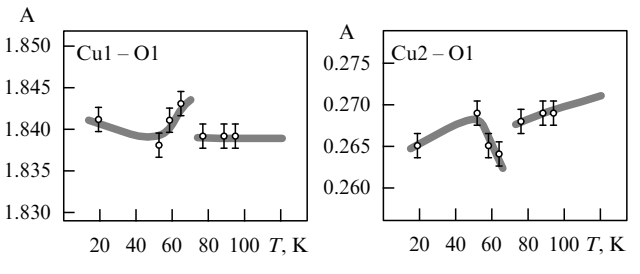

Figure 3. Behaviour of Cu1–O1 and Cu2–O1 interatomic distances in the structure of $YBa_2Cu_4O_8$ in the neighbourhood of the superconducting transition, $T_c = 72$ K.

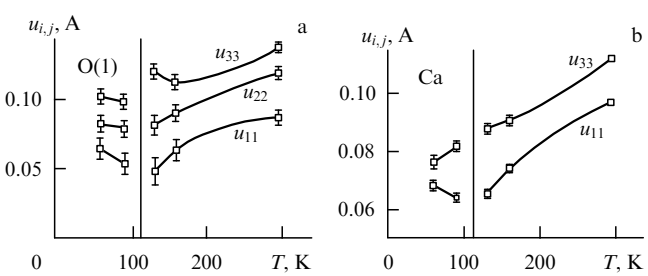

Figure 4. Behaviour of thermal vibrations of O1 and Ca atoms, characterized respectively by the general ellipsoid and the extended ellipsoid of revolution in the structure of $Tl_2Ba_2CaCu_2O_8$.

References

1. Simonov V I et al. *Pis'ma Zh. Eksp. Teor. Fiz.* **59** (4) 231 (1994) [*JETP Lett.* **59** 250 (1994)]; Molchanov V N et al. *Physica C* **229** 331 (1994)
2. Osiko V V *Fiz. Tverd. Tela* **7** (5) 1294 (1965) [*Sov. Phys. Solid State* **7** 1047 (1965)]; Aleksandrov V B, Garashina L S *Dokl. Akad. Nauk SSSR* **189** 307 (1969); Cheetham A K et al. *Solid State Commun.* **8** 171 (1970)
3. Muradyan L A, Maksimov B A, Simonov V I *Koord. Khim.* **12** (10) 1398 (1986)
4. Radaev S F, Simonov V I *Kristallografiya* **37** 914 (1992) [*Sov. Phys. Crystallogr.* (1992)]
5. Craig D C, Stephenson N S *J. Solid State Chem.* **15** 1 (1975)

PACS numbers: **75.30.–m**, 75.50.Pp

Quantum oscillations of resistance and magnetization in magnetic semiconductors and semimetals

A D Balaev, V V Val'kov, V A Gavrichkov, N B Ivanova, S G Ovchinnikov, V K Chernov

1. Quantum oscillations in the ferromagnetic semiconductor *n*-$HgCr_2Se_4$

Typically, Landau oscillations due to the electron orbit quantization in magnetic field give rise to oscillations, periodic in $1/H$, of the thermodynamic and kinetic characteristics of degenerate Fermi systems. Anomalous quantum oscillations are possible when the temperature and magnetic-field dependences of the chemical potential μ differ from the standard Fermi-liquid dependences, on account, e.g., of the effects of strong electron correlations. In this paper we present the experimental results on oscillations, weakly-periodic and aperiodic in $1/H$, of resistance and magnetization in single crystals of a degenerate ferromagnetic *n*-type semiconductor $HgCr_2Se_4$.

The ferromagnetic *n*-type semiconductor $HgCr_2Se_4$ has a temperature-independent electron concentration $n \sim 10^{18}$ cm^{-3} in the temperature range under investigation, $4.2\,\mathrm{K} < T < 77\,\mathrm{K}$, and possesses a high carrier mobility of the order of 10^3 cm^2 V^{-1} s^{-1} at 77 K, which enables the observation of Landau oscillations in fields of above 10 kOe. The non-Fermi-liquid effects in $HgCr_2Se_4$ are due to the existence of a localized chromium d-level Ω close to the bottom of the conduction band [1]. In a degenerate *n*-type semiconductor, the chemical potential μ is pinned near the d-level and weakly depends on the temperature T and on the magnetic induction H, and the bottom of the conduction band shifts proportionally to the magnetization $M(T, H)$. As a result, the dependence of the chemical potential $\mu(T, H)$ measured relative to the band bottom gains non-Fermi-liquid corrections. The magnetization oscillations with temperature in a similar many-electron model were calculated in Ref. [2], and, after publishing the experimental work [3], a more complete theory of the de Haas – van Alphen (dHvA) effect was recently developed in the work reported in Ref. [4]. According to the conclusions, the phase of the oscillatory part of the magnetization depends on the magnetic field as

$$\varphi = \frac{a}{H} + \frac{b}{\sqrt{H}}\,, \qquad (1)$$

where a and b are the constants independent of the field. As a result, the $1/H$ periodicity disappears, although the possibility of oscillations on account of the crossing of the Fermi level and the Landau level persists.

The magnetization of samples was measured using an automatic vibrational magnetometer with a superconducting solenoid in fields to 60 kOe [5] at a temperature of $T = 4.2$ K. The magnetic field was applied along the $\langle 100 \rangle$ crystal axis. The longitudinal magnetoresistance was measured using the four-probe technique. The oscillatory part of the resistance $R_\sim$ and the magnetization M are presented in Fig. 1 as functions of the magnetic field, and the inverse-field dependences of the resistance R and the magnetization are shown in Fig. 2. The data in Fig. 1a make it clear that the linear in-field magnetoresistance is superimposed on the oscillatory part of the resistance; we therefore represent $R(H)$ as

$$R(H) = R_\sim(H) - cH\,, \qquad (2)$$

where the parameter $c = R(60\ \mathrm{kOe}) \times 10^{-4}$ kOe^{-1}. The oscillatory part $R_\sim(H)$ separated in such a way is displayed in Fig. 1b. Comparison with the magnetic-field dependence of magnetization $M(H)$ in Fig. 1c reveals the coincidence of the extrema of the curves $R_\sim(H)$ and $M(H)$. As expected, the oscillations are periodic neither in H, nor in $1/H$. The spectral density of the signal shown in Fig. 2b has a smeared peak corresponding to an approximate period in $1/H$ of 0.8×10^{-6} Oe. However, it is possible to observe a distinct signal only in the field range $\Delta H = 8 - 20$ kOe (Fig. 3a). In stronger fields of $\Delta H = 20 - 60$ kOe, the amplitude of the first harmonic decreases, and, in turn, the number and amplitude of higher-frequency harmonics increase. As a consequence, the signal is 'absorbed' in the noise (Fig. 3b). From the known period we can find that the extreme cross-sectional area of the Fermi surface $S = 9.3 \times 10^{13}$ cm^{-2}, and of the carrier concentration $n \sim 4.3 \times 10^{18}$ cm^{-3}.

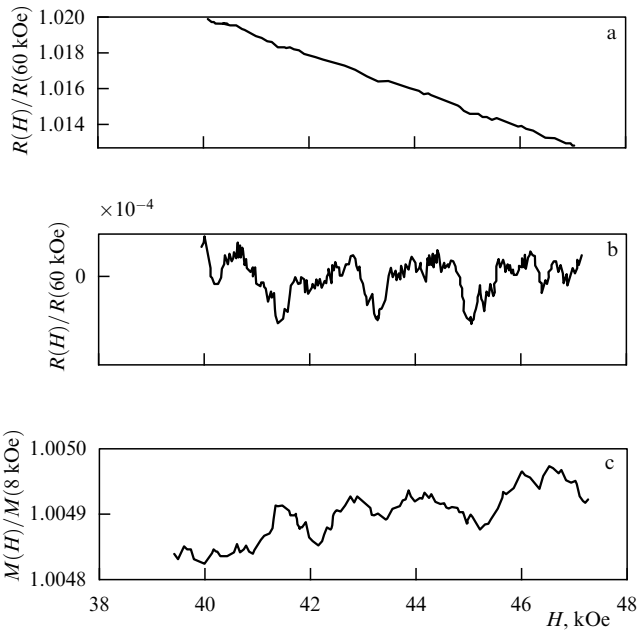

Figure 1. Magnetic-field dependence of the full resistance (a), the oscillatory part of the resistance (b), and the relative magnetization (c) in the degenerate *n*-type semiconductor $HgCr_2Se_4$, measured at $T = 4.2$ K.

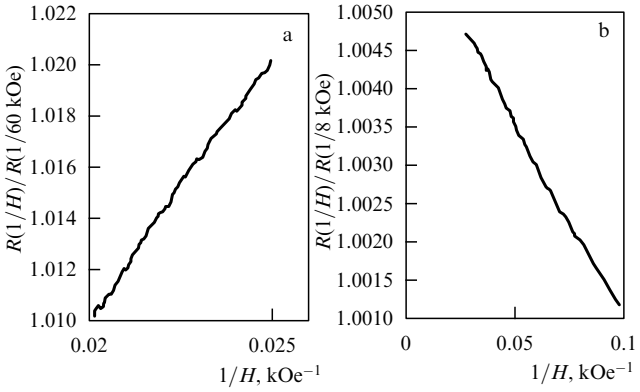

Figure 2. Inverse-field dependence of the oscillatory part of the resistance (a) and magnetization (b) in the degenerate *n*-type semiconductor $HgCr_2Se_4$ at $T = 4.2$ K.

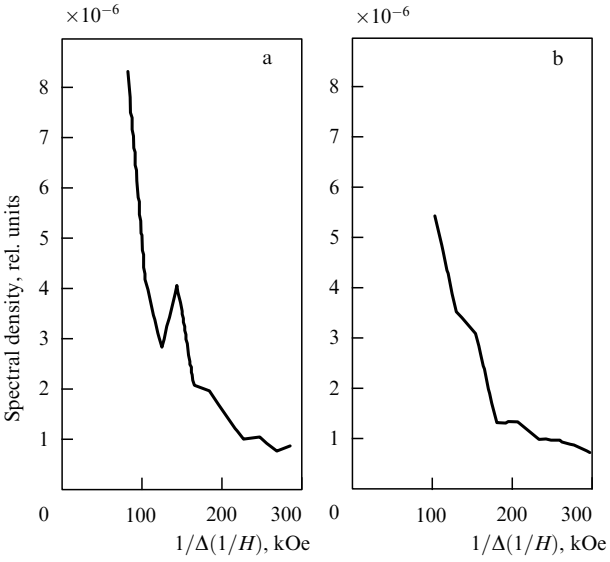

Figure 3. Spectral density of magnetization $M(1/H)$ in the field range 8–20 kOe (a) and 20–60 kOe (b).

The relative amplitudes of oscillations are not large, $\sim 10^{-4}$, but they exceed by an order of magnitude the error of the magnetization measurement [5]. The smallness of the amplitude of magnetization oscillations is due to the carrier concentration trifle, since with $n \sim 10^{18}$ cm^{-3} the number of electrons per cell is about 10^{-4}. The relative amplitude of resistance oscillations exceeds it by approximately a factor of five.

Calculation of the magnetic semiconductor magnetoresistance [6] in the framework of a many-electron model at low temperatures shows that the dependence $R(H, T)$ makes itself evident through the dependence $M(H, T)$, in accordance with the exact coincidence of the extrema in Fig. 1b and 1c. The scattering by impurities and intrinsic defects in the lattice is a predominant mechanism for resistance. The residual resistance turns out to be dependent on the temperature and on the magnitude of the magnetic field. Our results coincide surprisingly well with the studies of temperature and field dependences in lanthanum-manganese perovskites ABO_3, where the dependence $R(H)$ has been also proved to be determined by the magnetization dependence of resistance $R\big(M(H)\big)$ [7]. The coincidence of our conclusions with those of this work is, perhaps, not accidental: the narrow-band quasi-particles with properties due to strong electron correlations are charge carriers in either case.

Contrary to normal Fermi-liquid systems where the weak temperature dependence of the chemical potential $\mu(T) = \varepsilon_F + T^2/\varepsilon_F$ leads to the temperature damping of quantum oscillations with the well-known Kosevich factor $T/\sinh(T)$, in our case, owing to the strong temperature dependence of the sd-exchange splitting of spin subbands, as well as to the pinning of the chemical potential by the d-level, the chemical potential itself (measured relative to the band edge) gains a strong temperature dependence [4]. As a consequence, with varying temperature a crossing of the chemical potential μ with the Landau levels may be observed. We have made such measurements in Ref. [3]. The experimental value of the oscillatory part of the magnetization was determined as the difference between the experimental value of magnetization and the spin-wave contribution to the magnetization. Figure 4 displays the experimental and theoretical temperature dependences of the oscillatory part of magnetization at $H = 60$ kOe. The revealed oscillations of the magnetization are damped out with temperature, with the characteristic period $\Delta T \approx 40$ K.

Thus, the Shubnikov–de Haas (ShdH) and dHvA effects in the degenerate ferromagnetic *n*-type semiconductor $HgCr_2Se_4$ may be observed for fields $H = 8-60$ kOe, but their field dependence is not described in terms of the $1/H$-periodic functions, traditional for the Fermi liquid.

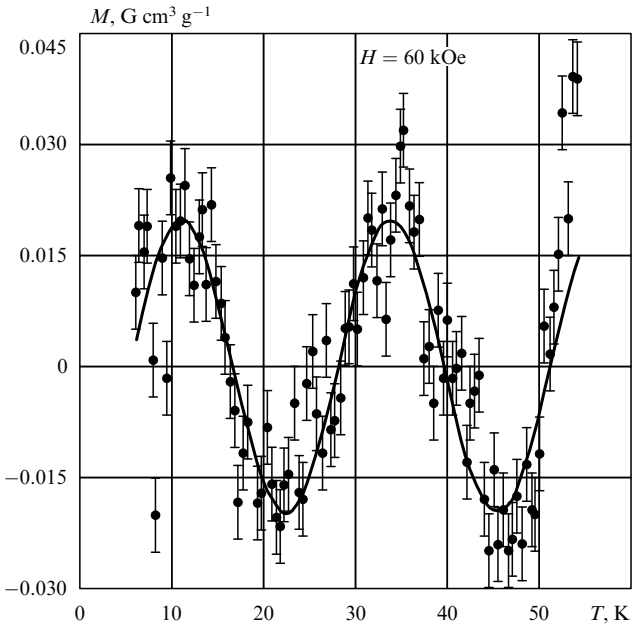

Figure 4. Temperature dependence of the oscillatory part of the magnetization in an *n*-type semiconductor $HgCr_2Se_4$ at $H = 60$ kOe [3]. The dots show the experimental dependence, and the solid line represents the theoretical results.

2. De Haas–van Alphen effect in a narrow-band antiferromagnetic semimetal

The nontriviality of the ground-state electronic structure of strongly correlated systems has stimulated more active

studies on the dHvA effect in heavy-fermion compounds [8–10], high-temperature superconductors [11, 12], as well as in antiferromagnetic compounds with low charge-carrier concentrations [13, 14]. A dHvA experiment in $CeCu_2Si_2$ [10] exhibited the essential role played by long-range antiferromagnetic ordering in the formation of dHvA oscillations. The measurements were carried out in the range of magnetic fields H stronger than the field H_{c2}, as the compound was in the normal phase. A dramatic change in the period of the oscillatory dependence of magnetization in passing through the critical field H_c was clearly observed. The field H_c corresponded to the point of the spin-flip transition, in which the antiferromagnetic vector vanished. The influence of magnetic order on the dHvA effect has been considered in Refs [15, 16]; the change of the oscillation period in going through the spin-flip point, however, was not discussed.

The case of valence-band states capable of forming magnetopolaron states is of particular interest, when strongly-correlated conducting antiferromagnets with low charge-carrier concentrations are considered. Such a situation seems to be realized in cerium monopnictides [13, 14]. The magnetopolaron states formed on account of s–f exchange coupling between the spin moments of the localized subsystem and the valence-band holes are responsible for the band narrowing (the effective mass enhancement) [17]. In a magnetic field H, when the noncollinear phase of the antiferromagnet with canted sublattices is realized, the band narrowing becomes strongly dependent on H. Such a situation persists up to the spin-flip transition point, when the transformation of the magnetic structure is completed with the appearance of ferromagnetic ordering. A key physical peculiarity in the behaviour of such an antiferromagnet in strong magnetic field involves two points. Firstly, Landau quantization arises, and additional oscillatory contributions to the magnetization of itinerant charge carriers appear. Secondly, the dHvA effect occurs in the conditions of a dramatic rearrangement of the system ground state, induced by the magnetic field itself. These factors make possible a drastic change in the period of dHvA oscillations in passing through the spin-flip point. For simplicity, we restrict our consideration to the case of s–f exchange coupling valid only for holes, with the conduction electrons unbound to the localized subsystem.

The solution to the problem of the magnetopolaron spectrum of a narrow-band antiferromagnet in the canted phase [18] and the use of the charge-neutrality condition of a semimetal lead to the conclusion that the rate of motion of the upper Landau levels is strongly renormalized as the magnetic field changes. In this case, the depletion of the upper Landau levels typical of dHvA effect occurs to the right of the spin-flip transition point as they cross the chemical potential with increasing field H. To the left of the transition point, however, the picture is completely different. The increase in H causes such a rapid growth of the charge carrier concentration that despite the increasing energy separation between the Landau levels, the occupation of the new Landau levels none the less occurs. The rate of such a 'renormalized' process is determined by the concentration at the spin-flip transition point, the growth rate of the number of occupied Landau levels to the left of H_c being less, equal to or more than that of the depletion of the upper Landau levels to the right of H_c. This suggests three behaviour regimes for the period of dHvA oscillations in passing through H_c.

Figure 5 shows a typical dependence of the oscillatory part of the band electron magnetization in an antiferromagnetic compensated semimetal with magnetopolaron hole states in the vicinity of the spin-flip transition. The band carrier concentration n is less than the critical value n_c that in our case is 6.2×10^{-3} cm^{-3}. In this instance, the oscillations occur more often at $H < H_c$ than at $H > H_c$. If $n > n_c$, the inverse situation does take place: to the left of the spin-flip transition point the period of oscillations is larger than to the right. This situation is demonstrated in Fig. 6. At $n = n_c$, a third behaviour regime of the dHvA oscillations is realized in the neighbourhood of the spin-flip point, namely, the period of oscillations remains unchanged at the transition.

The authors would like to thank T G Aminov, A E Zhukov, V M Novotortsev and G I Shabunina for providing the facilities to investigate $HgCr_2Se_4$ single crys-

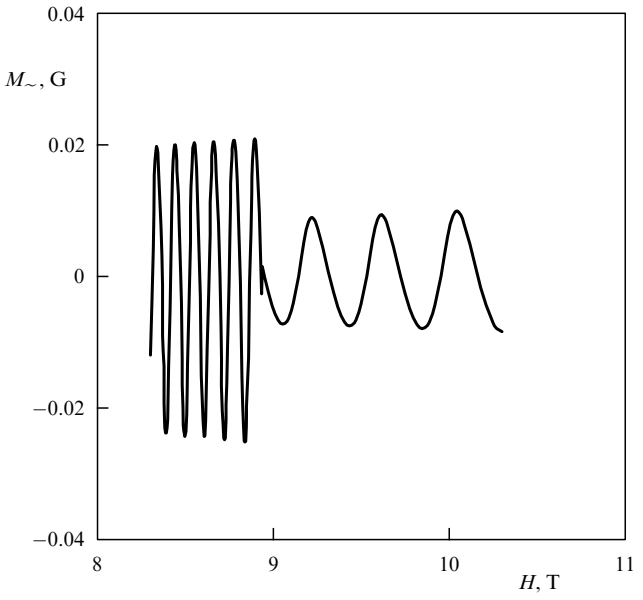

Figure 5.

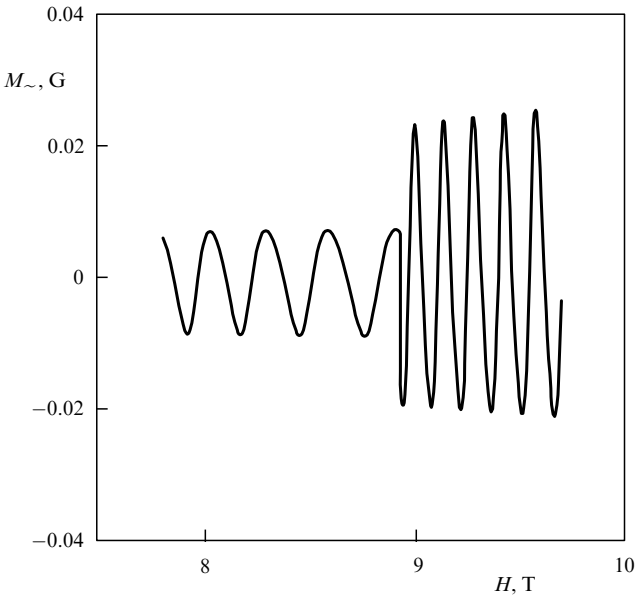

Figure 6.

tals, obtained in the N S Kurnakov Institute of General and Inorganic Chemistry, RAS, Moscow. We are also grateful to the Russian Foundation for Basic Research (Grant No. 96-02-16075) for financial support.

References

1. Gavrichkov V A, Erukhimov M Sh, Ovchinnikov S G *Fiz. Tverd. Tela* (Leningrad) **29** 527 (1987) [*Sov. Phys. Solid State* **29** 298 (1987)]
2. Val'kov V V, Ovchinnikov S G *Fiz. Tverd. Tela* (Leningrad) **24** 1801 (1982) [*Sov. Phys. Solid State* **24** 1024 (1982)]
3. Ovchinnikov S G et al. *Pis'ma Zh. Eksp. Teor. Fiz.* **62** 620 (1995) [*JETP Lett.* **62** 642 (1995)]
4. Val'kov V V, Dzebisashvili D M *Zh. Eksp. Teor. Fiz.* **111** 654 (1997) [*JETP* **84** 360 (1997)]
5. Balaev A D et al. *Prib. Tekh. Eksp.* **28** (3) 167 (1985) [*Instrum. Exp. Tech.* **28** 685 (1985)]
6. Gavrichkov V A, Ovchinnikov S G *Semicond. Sci. Tech.* (1997) (in press)
7. O'Donnell J et al. *Phys. Rev. B* **54** R6841 (1996)
8. Reinders P H P et al. *Phys. Rev. Lett.* **57** 1631 (1986)
9. Taillefer L, Lonzarich G G *Phys. Rev. Lett.* **60** 1570 (1988)
10. Hunt M et al. *J. Phys.: Condense. Matter* **2** 6859 (1990)
11. Fowler C M et al. *Phys. Rev. Lett.* **68** 534 (1992)
12. Bykov A I et al. *Pis'ma Zh. Eksp. Teor. Fiz.* **61** 101 (1995) [*JETP Lett.* **61** 106 (1995)]
13. Kasuya T, Suzuki T, Haga Y *J. Phys. Soc. Jpn.* **62** 2549 (1993)
14. Kasuya T *J. Phys. Soc. Jpn.* **64** 1453 (1995)
15. Rusul J W, Schlottmann P *Physica B* **163** 689 (1990)
16. Sollie R, Schlottmann P *Phys. Rev. B* **41** 8860 (1990)
17. Nagaev É L *Fizika Magnitnykh Poluprovodnikov* (Physics of Magnetic Semiconductors) (Moscow: Nauka, 1979) [Translated into English (Moscow: Mir, 1983)]
18. Val'kov V V, Dzebisashvili D M *Fiz. Tverd. Tela* (St.-Petersburg) (in press)

PACS number: **61.46.+w**

New crystalline and amorphous carbon modifications produced from fullerite at high pressure

V V Brazhkin, A G Lyapin, S G Lyapin, S V Popova, R N Voloshin, Yu A Klyuev, A M Naletov, N A Mel'nik

This report concerns the study of dense carbon modifications produced from the fullerites C_{60} and C_{70} and higher fullerites C_{2N} $(50 < 2N < 170)$ at high pressures and high temperatures. There are at least two points which make these investigations interesting for a broad scientific audience.

Firstly, the physics and chemistry of fullerites is a rapidly developing and extremely promising branch of knowledge. At ambient pressure, C_{60} fullerites are soft crystals characterized by a weak van der Waals interaction between molecules, with a density of about 1.6 g cm^{-3} and a bulk modulus $B \approx 18$ GPa [1]. By treating fullerites with elevated pressures and temperatures, it is possible to synthesize a whole spectrum of crystalline and disordered carbon phases with densities lying in the range from 'fullerite' to 'diamond' values and with high mechanical characteristics [2–7]. To date, the production and investigation of these novel carbon modifications have been reported in dozens of publications.

The second point is related to sensational statements in both scientific journals and popular science literature [6, 8, 9], as well as in the mass media that some dense carbon phases obtained on the basis of C_{60} possess a higher hardness than diamond. The possibility of producing phases from fullerites with higher elastic moduli than those of diamond has been associated with the high mechanical stability of a single C_{60} molecule [10, 11].

These two aspects motivated this contribution. It deals firstly with a description of the most dense carbon modifications obtained from fullerites, and secondly with an analysis of their mechanical properties.

At relatively low pressures (up to 1 GPa), the fullerites C_{60} and C_{70} exhibit orientational transitions and the 'freezing' of molecular rotation in a similar way as they do with decreasing temperature at ambient pressure. At higher pressures and elevated temperatures (1200–2000 °C), C_{60}, C_{70} and C_{2N} are transformed to carbon modifications with stability regions in the phase graphite–diamond diagram. The transformations occur through intermediate metastable phases. At pressures of 1–8 GPa and temperatures of 150–900 °C, 1D- and 2D-polymerized phases are formed from covalently bonded C_{60} molecules [2–4]. The density of these phases ranges from 1.8 to 2.5 g cm^{-3}. The formation of covalent bonds between particular molecules seems to occur by means of the [2 + 2] cyclo-addition mechanism [12].

At pressures above 9 GPa and temperatures over the range $20 < T < 600$ °C, 3D-polymerized phases form, with C_{60} molecules covalently bonded in all directions [5–7]. Such phases may be considered as a partially ordered 3D covalent network of carbon atoms with a particular share of sp^2 and sp^3 states. Until recently, these dense ($\rho \sim 2.4$–3.1 g cm^{-3}) modifications were less thoroughly studied than the 1D- and 2D-polymerized phases. At higher temperatures, the various polymerized phases transform to the amorphous carbon state with a variable share of sp^2 and sp^3 configurations depending on the pressure [5, 6, 13] which, in turn, crystallizes to diamond or graphite.

We have mainly studied the processes of 3D C_{60} polymerization and subsequent transformation to amorphous sp^2–sp^3 carbon on heating at a pressure of 12.5 GPa. Figures 1 and 2 present the X-ray diffraction data and the Raman spectra of samples corresponding to different heating temperatures.

As the temperature of treatment is increased over the range 20 to 400 °C, the degree of polymerization increases to the complete polymerization, with any one of these molecules being covalently bonded to each of the twelve surrounding molecules. Upon further heating, the shape of molecules is distorted, and the mechanisms for additional polymerization seem to be triggered, the density increasing from 2.7 to 3.1 g cm^{-3}. Heating to 500 °C and above leads to the complete destruction of the molecules and a transition to an amorphous carbon phase with a density of 3.0–3.2 g cm^{-3}. The Raman spectra of crystalline phases with high degrees of polymerization give evidence for a significant disorder, perhaps, of orientational nature, in the formation of covalent bonds between molecules. The Raman spectrum of the amorphous phase (500 °C) is close to those of amorphous carbon films with a large share of atomic sp^3 states (70–90%). The continuous change of the fullerite fcc-lattice parameter after heating at high pressure (> 9 GPa) may be explained by means of the 3D-polymerization model [7] that treats partially polymerized phases as a solid solution of van der Waals and covalent bonds. At the same time, the appearance of 1D- and 2D-polymerized phases at lower pressures may be interpreted as an ordering ('crystalliza-

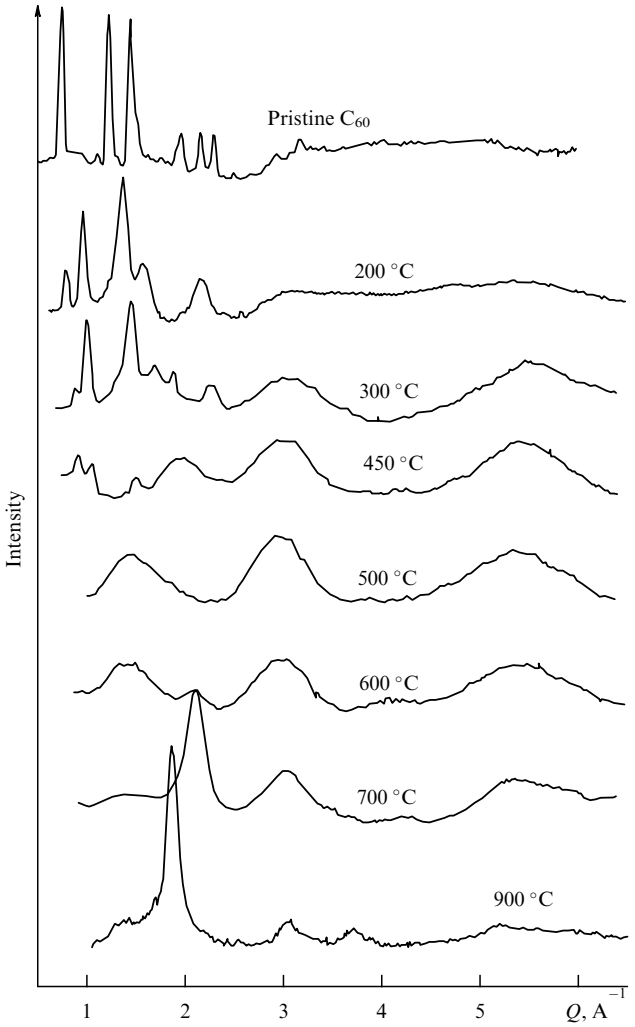

Figure 1. X-ray structural data for carbon phases obtained after heating of C_{60} at 12.5 GPa ($Q = 4\pi \sin\theta/\lambda$, where 2θ is the scattering angle of X-rays with wavelength λ).

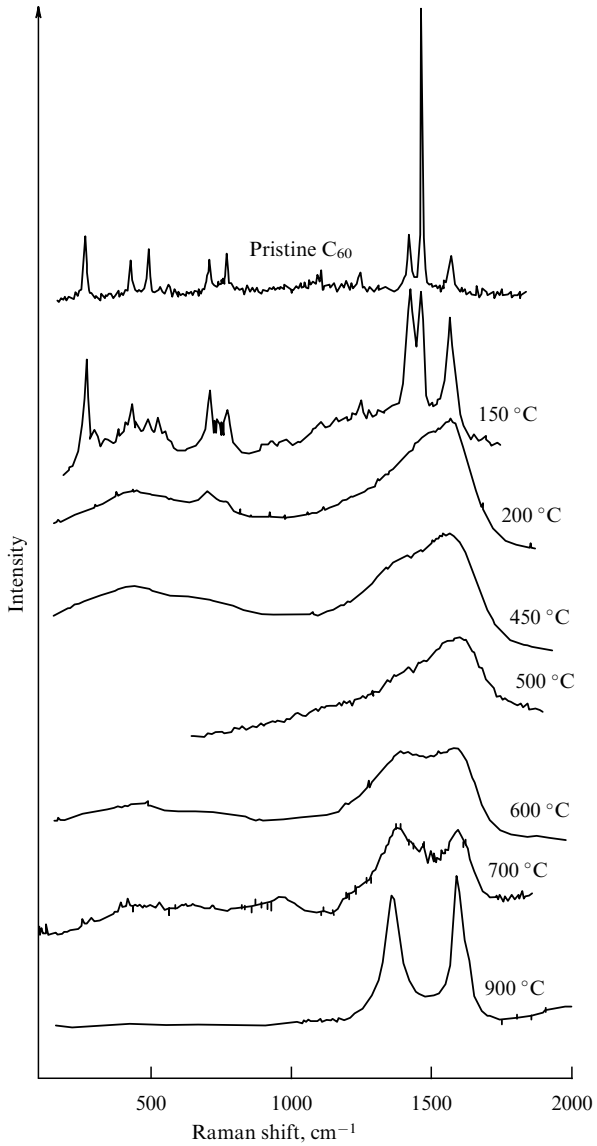

Figure 2. Raman spectra of the samples produced from C_{60} at 12.5 GPa.

tion') of covalently bonded molecular pairs along the planes or chains of polymerization.

We have also carried out preliminary investigations of the behaviour of C_{70} and C_{2N} fullerites on heating at pressures of 8 and 12.5 GPa. At 8 GPa, 1D polymerization in C_{70} crystals is observed from 300 to 500 °C. At $T > 600$ °C, the destruction of molecules and the formation of a graphite-like amorphous phase with a density of 2.3 g cm^{-3} occur. At the pressure of 12.5 GPa, the formation of the amorphous phase with a large share of sp^2 states begins even at 300 °C, i.e. fullerite C_{70} is less stable than C_{60}, apparently due to the non-spherical shape of C_{70} molecules. When heated under pressure, higher fraction C_{2N} fullerites also change into an amorphous carbon state with a density between 1.9 and 2.4 g cm^{-3}.

The mechanical properties of the dense carbon phases involved are of special interest. The data on the Young's modulus, hardness and fracture toughness of the samples synthesized are given in Table 1. It is evident that the Young's modulus and hardness of the phases obtained are 1.5 – 4 times less than the corresponding figures for diamond, whereas the fracture toughness and plasticity can even exceed those of diamond. A well-defined correlation is observed between the mechanical characteristics (the Young's modulus and hardness) and the density of phases or shares of atomic sp^3 configurations (Fig. 3).

Similar dependences of the Young's modulus on the share of sp^2 states (or on the density) have been found using

Table 1. Experimental density ρ, hardness H_V, fracture toughness K_{1c}, and Young's modulus E for some carbon phases obtained after the treatment of C_{60}, C_{70} and C_{2N} fullerites at high pressure (P_{syn}) and high temperature (T_{syn}).

Fullerite	P_{syn}, GPa	T_{syn}, °C	ρ, g cm^{-3}	H_V, GPa	K_{1c}, MN m$^{-3/2}$	E, GPa
C_{60}	12.5	300	2.6	36 ± 7	plastic	350
		400	2.8	26.4 ± 0.7	plastic	400
		450	3.0	52 ± 6	7.9 ± 1.4	
		500	3.15	76 ± 1	15 ± 4	700
		650	2.9	73 ± 5	7.6 ± 1.2	
		900	3.0	87 ± 10	8.2 ± 1.8	
C_{70}	8.0	600	2.2	9.4 ± 2.0	3.7 ± 0.2	
C_{2N}	12.5	500	2.0	21 ± 1.5	plastic	
	12.5	600	2.1	24.6 ± 2.2	4.3 ± 1.5	

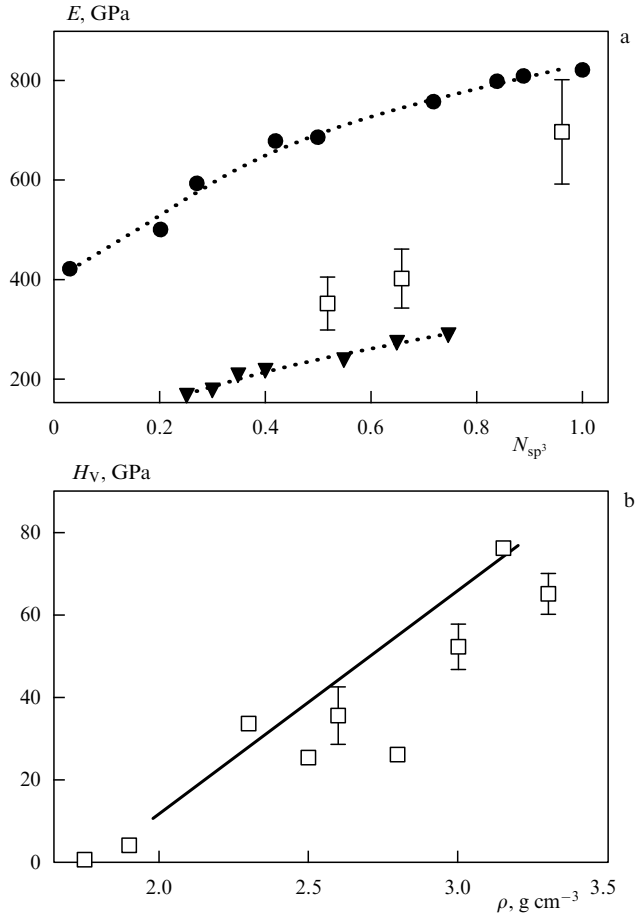

Figure 3. Comparison of experimental data (squares) obtained for Young's modulus (a) and hardness (b) with the results for amorphous carbon known theoretically [14] (circles) and experimentally [15] (triangles in (a) and the interpolation line between the experimental points in (b) are taken from Ref. [15]).

computer simulation of amorphous carbon sp^2-sp^3 networks [14] and by studying deposited amorphous carbon films [15] (see Fig. 3). Such a correlation may be understood from the analysis of various contributions to the cohesive energy of a solid. In the general case, the density dependence of elastic moduli can be rather complicated but, in the arrangements of identical atoms with bonds of a similar type, all the elastic moduli may be thought of as depending monotonically on the density.

Carbon with a particular share of sp^2 states both in ordered and disordered phases possesses a lower density and elastic moduli than diamond. Among bulk carbon materials, the phases with R8, BC8, β-Sn, simple cubic and some other structures may have higher densities than diamond [16, 17]. In these structures, the inner deep-lying *s*-electrons are partially involved in the formation of chemical bonds. As a result, these structures become stable only at pressures of the order of 10^3 GPa, and the question of the existence of such phases in a metastable state under ambient conditions calls for further investigation.

Notice that in the case of a perfect crystal without defects, such technological parameters as hardness and strength are bound to be comparable in magnitude to the elastic moduli. Only the elastic moduli are of physical interest, since other mechanical characteristics depend on both the sample morphology and the measurement technique. From this point of view, the well-known statement that diamond is the hardest material in nature is not too informative. No wonder that in particular tests under certain conditions, a number of substances, amorphous diamond-like carbon being among them, may be harder than diamond. For instance, at temperatures exceeding 1000 °C, diamond becomes less hard than silicon carbide SiC. The statement that of all known substances diamond possesses the highest elastic moduli is more physically informative. This mainly concerns the shear modulus, whose uniquely high value ($\sim$ 5 Mbar) results in the outstanding mechanical properties of diamond, including its hardness.

Thus, the dense modifications produced from fullerites at high pressure represent a new class of both crystalline ordered and disordered sp^2-sp^3 carbon phases. These phases are intermediate in density and mechanical properties between pure sp^2 (fullerite, graphite) and sp^3 (diamond, lonsdaleite) modifications. Previously, it was possible to obtain carbon phases with a gradually changing share of valent sp^2 and sp^3 states only in amorphous thin films. The unique combination of rather high hardness, plasticity and fracture toughness (see also Ref. [5]) makes these carbon materials very promising. The optical and electron transport properties of the novel carbon phases obtained are the subject of further research.

In this work, the maximum pressure was limited by the capabilities of the experimental equipment used for the high-temperature synthesis of bulk samples. However, the series of irreversible transformations observed in fullerite C_{60} at $P = 12.5$ GPa seems to be common at high pressures ($P > 9$ GPa) and high temperatures. Indeed, the experimental evidence [13, 18, 19] does show that the compression of C_{60} at room temperature initiates structure transformations similar to those observed in this study at high temperatures (but at a somewhat lower pressure). Structural investigations of the transformations made directly under high pressure could provide additional information on the mechanisms of polymerization and disordering in C_{60} and other fullerites.

This work was supported by the Russian Foundation for Basic Research (Grants Nos. 96-02-17328a and 95-02-03677).

References

1. Duclos S J et al. *Nature* (London) **351** 380 (1991)
2. Iwasa Y et al. *Science* **264** 1570 (1994)
3. Núnez-Regueiro M et al. *Phys. Rev. Lett.* **74** 278 (1995)
4. Marques L et al. *Phys. Rev. B* **54** R12633 (1996)
5. Brazhkin V V et al. *Pis'ma Zh. Eksp. Teor. Fiz.* **62** 328 (1995) [*JETP Lett.* **62** 350 (1995)]
6. Blank V D et al. *Phys. Lett. A* **205** 208 (1995)
7. Brazhkin V V, Lyapin A G, Popova S V *Pis'ma Zh. Eksp. Teor. Fiz.* **64** 755 (1996) [*JETP Lett.* **64** 802 (1996)]
8. Blank V D et al. *Zh. Tekh. Fiz.* **64** 153 (1994) [*Sov. Phys. Tech. Phys.* **39** 828 (1994)]
9. Blank V D, Buga S G *Nauka i Zhizn'* **10** 61 (1995)
10. Ruoff R S, Ruoff A L *Nature* (London) **350** 663 (1991); *Appl. Phys. Lett.* **59** 1553 (1991)
11. Wang Y, Tomanek D, Bertsch G F *Phys. Rev. B* **44** 6562 (1991)
12. Goze C et al. *Phys. Rev. B* **54** R3676 (1996)
13. Hodeau J L et al. *Phys. Rev. B* **50** 10311 (1994)
14. Kelires P C *Phys. Rev. Lett.* **73** 2460 (1994)
15. Weiler M et al. *Phys. Rev. B* **53** 1594 (1996)
16. Clark S J, Ackland G J, Crain J *Phys. Rev. B* **52** 15035 (1995)
17. Biswas R et al. *Phys. Rev. B* **35** 9559 (1987)
18. Moshary F, Chen N H, Silvera I F *Phys. Rev. Lett.* **69** 466 (1992)
19. Snoke D W, Raptis Y S, Seassen K *Phys. Rev. B* **45** 14419 (1992)

PACS numbers: 12.20.Fv, **11.30.–j**, **03.30.+p**, 06.30.Gv

An experimental study of the optical isotropy of space

V V Ragul'skiĭ

According to modern theoretical concepts, the surrounding space is isotropic relative to optical phenomena. This makes one think (see, for example, Ref. [1]) that the refractive action of condensed matter on light waves propagating in opposite directions is totally identical†. However, the experimental foundations for such considerations are quite insufficient.

The point is that the direct comparison of the refractive properties of matter for oncoming light beams has so far been made with an accuracy no better than $\sim 3 \times 10^{-5}$ (see Arago's paper [3]). As follows from the results published in that paper, the refractive index n of glass does not depend, within this uncertainty, on whether the light source is ahead of the orbital motion of the Earth or this source gives light in pursuit of it.

Papers are also known [4, 5] reporting changes in the polarization of oppositely directed beams passing through a tilted glass plate. The corresponding refractive indices were calculated using the data obtained and Fresnel's formulae. These works are close to each other in methodics but opposite by their results. As follows from Fizeau's data [4], if one of the beams propagates East and another West, *the* '*opposite*' *refractive indices differ* from each other, with the difference (Δn) depending on the time and reaching 3×10^{-4}. However Brace [5], using his own measurements (the uncertainty of which is equivalent to $\Delta n \sim 4 \times 10^{-5}$), stated that the 'eastern' and 'western' *refractive indices are the same*.

Generally speaking, it is not excluded that different factors affect the isotropy of the observed optical processes. For example, the authors of the cited papers admitted that a rapid motion may have an effect. As is well known, the theory of relativity postulates the absence of such a dependence, but postulating is not proving.

As shown above, the experimental results on light refraction are already in disagreement with each other in the fourth decimal figure. To clarify the situation, an experiment [6] was carried out.

The principal elements of the experimental installation are shown in Fig. 1. The electric lamp L is a light source shining on a narrow slit S in the focal plane of the objective O_1. The parallel beam formed by the objective is refracted by the prism V and enters the high quality triple-prism T. It is well known that such a reflector turns the incident light beam by 180° independently of the incident angle. The reflected light passes through the prism V in the opposite direction and is brought to a focus by the objective O_1. Then some light fraction goes out through a semitransparent mirror M_1, thus separating from the initial radiation.

A thin line is engraved on the surface of the plane-parallel plate R to determine the angular position of the beam passing through the prism twice. The plate is located in the plane where the beam, being focused, forms an image of the slit S. The plate is secured on a carriage, which can be shifted with a micrometric mechanism. All the elements are installed on the platform P allowing rotation of the apparatus as a whole without rearrangement.

† In particular, this assumption is widely used in the theory and practice of optical phase conjugation (see, for example, Ref. [2]).

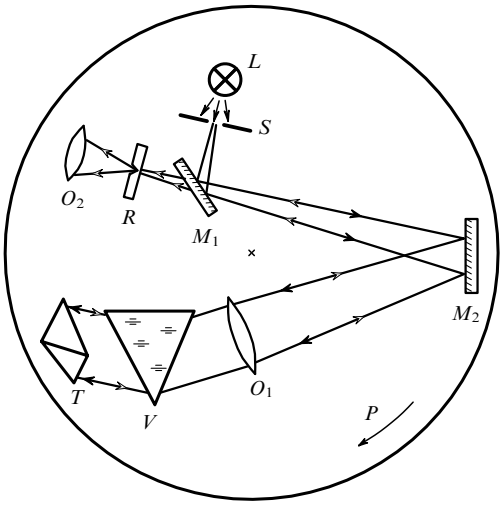

Figure 1. Experimental scheme to determine the refractive index isotropy: L — an electric lamp; S — a slit 10 μm wide; O_1 — an achromatic objective with focal length 1.5 m; V — a prism of K-8 glass with refracting angle 65°; T — a glass triple-prism, which reflects a light beam 5 cm in diameter; M_1 — a plane semitransparent mirror with an antireflection coating on the back side; M_2 — a plane mirror with an opaque aluminium coating; R — a moving glass plate with a right line of 3 μm width; O_2 — an ocular with 100-fold magnification; P — a turning platform.

A nonzero Δn would shift the image by Δx. An elementary calculation shows that these quantities are related as

$$\Delta n = \frac{\sqrt{1 - n^2 \sin^2(0.5\gamma)}}{2f \sin(0.5\gamma)} \Delta x \,, \qquad (1)$$

where γ is the prism's refracting angle, f is the focal distance of the objective O_1. For the known parameters of the apparatus ($\gamma = 65°$, $n = 1.52$, $f = 1.5 \times 10^2$ cm) we obtain $\Delta n = 3.6 \times 10^{-3}$ [cm^{-1}] Δx [cm].

Preliminary tests show that the angular position of the beam under consideration is best observed by the diffraction picture that appears when the beam shines at the marker line. A symmetry of this picture observed at a distance of 0.5 mm from the marker through the ocular O_2 is so sensitive to the transverse shifts of the marker with respect to the centre of the falling light field (whose width is comparable with that of the marker) that shifts as small as 0.1 μm are quite detectable.

With the technique described above, the value of Δx was found for 18 positions of the platform spaced by 20°. In each of them, 10 micrometric counts were read at which the marker line coincided with the centre of the slit image. The result was that for all orientations of the platform the deviation of the parameter measured from zero is within the root-mean-square uncertainty, which is 5×10^{-8} in units of Δn. Thus it follows that the laboratory space is isotropic relative to light refraction at least to such an accuracy.

The refractive index is determined by the ratio of the velocity of light propagation inside matter to that in the surrounding medium. Therefore, the result obtained means that both these velocities are either isotropic or depend similarly on direction.

Presently, the speed of light has been measured to an accuracy of 1 m s^{-1} (see Ref. [7]). But in all precise experiments, *the speed averaged over two opposite directions*

were determined [8] (for example, by measuring the time it takes for light to travel two times a fixed distance – from the source and back). Experimental works, which can provide information on the '*one-direction*' velocity, demonstrate a huge variety of results. For example, according to Ref. [9] this velocity differs from the mean value (c) by no more than 1 km s^{-1}, if any. But in Ref. [10], it is stated that the difference (Δc) between these velocities reaches 360 ± 40 km s^{-1} for some azimuthal angles. Such a diversity makes one look for new more precise experiments for measuring the one-direction speed of light.

The idea of a recent experiment [11] performed by myself consists in separating the paths that the light travels from the source and back, and making the time the light takes along each way different by embedding one of them in a medium with a nonunitary refractive index. The asymmetry of the paths causes the total time for the light to propagate along them, for $\Delta c \neq 0$, to depend on their spatial orientation. Let the phase speed of the light during its propagation from the source be $c + \Delta c$. Then for the opposite direction it is $c - \Delta c$. Clearly, in order to propagate along the two paths of length l each, the light wave will take a time

$$t_1 = \frac{l}{c + \Delta c} + \frac{n_1 l}{c - \Delta c}\,, \tag{2}$$

where n_1 is the refractive index of the medium for this wave.

Changes in the time t_1, depending on the trajectory orientation, can in principle be measured by interferometry. To do this, one needs to release a similar light wave by the same closed route but in the opposite direction. The expression for its travel time (t_2) differs from t_1 (2) by the sign before Δc and, generally, by the refractive index, which is n_2 for such a wave. Taking this into account, the time difference is

$$\Delta t \equiv t_1 - t_2 = \frac{2(n-1)l\Delta c - cl\Delta n}{c^2 - (\Delta c)^2}\,. \tag{3}$$

Here $n \equiv (n_1 + n_2)/2$ and $\Delta n \equiv n_2 - n_1$. Thus, if the wavefronts of the waves under consideration initially coincide, after having passed the closed route they turn out to be separated by a distance linear in Δc [the value $(\Delta c)^2$ in the denominator (3) may of course be neglected], which must affect the interference picture formed by these waves.

The scheme of an experimental setup, in which such idea is realized [11], is presented in Fig. 2. Its principal element is a ring interferometer formed by a thick plane-parallel plate P and the triple-prism T. A glass sample G is inserted inside it. The interferometer works as follows. Several mutually parallel beams form (due to refraction and reflection of the light by its boundaries) from laser radiation falling at some angle on the plate, two of which then enter the triple-prism. This angular reflector is set up such that its top is in the midpoint between the two beams. As a result, the reflected beams not only turn by 180°, but also became interchanged: the beam entering the triple-prism by the upper path is directed to the plate by the bottom way, and vice versa. Thus two light waves emerge, one of which travels the closed route clockwise and the other anticlockwise. The plate then joins the returned waves together, after which they propagate toward the laser L by interfering with each other. All elements are installed on a turning platform.

The interferometer described above is extremely stable relative to vibrations and deformations of the array (which inevitably occur during its turns), since positional shifts of its components do not affect the angle between the interfering beams and their time delay. But this angle does depend on the characteristics of the optical elements used. In the present work, a triple-prism with slightly nonorthogonal faces was selected. This causes a slight angular divergence to appear during the reflection of two parallel beams from the prism. This difference is 6×10^{-4} rad in our experiment. It could be compensated for (or increased) by turning a wedge-like plate V with a refracting angle of 5×10^{-4} rad. Thus, one can widely vary the distance between interference fringes that appear during the wave superposition at the interferometer exit. The registration of these fringes is made with a moving slit S.

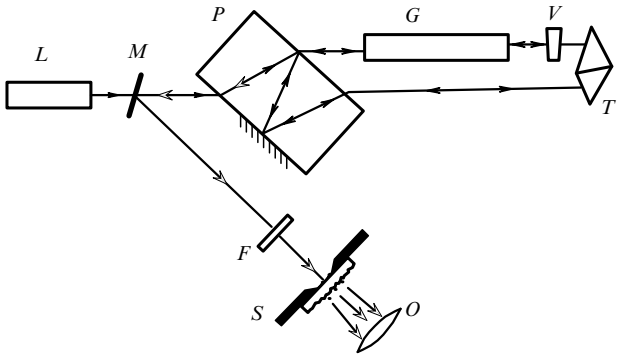

Figure 2. Optical scheme of the device for checking the isotropy of light velocity: L — a single-mode He – Ne laser; M — a semitransparent mirror; P — a plane-parallel plate of melted quartz 4 cm wide, with a mirror coating on part of its surface; G — a glass rod 68 cm in length with plane-parallel ends; V — a wedge-like glass plate; T — a triple-prism, i.e. a corner reflector in the form of a cut corner of a cube; F — a film polarizer; S — a movable slit with a width of 0.2 mm and the adjacent mat-lavsan-film diffuser; O — an ocular with 15-fold magnification.

The experiment demonstrated that when the distance h between the minima in the interference picture is 7 mm, the positioning of the slit is made to an accuracy of 3 μm. As is known, the shift of such a picture by an amount h corresponds to a change by λ in the distance between the fronts of the interfering beams, where λ is the wavelength of the light involved. Thus, the relative position of these fronts in the device under discussion was controlled with a precision of $\lambda/2000$.

It is easy to understand how the positional shift of minima Δh relates to the observable value Δc. According to the above calculations, the space gap between the fronts of the interfering waves is $c\Delta t$. Consequently, it is equal to $c\Delta t/\lambda$ in units of wavelength, which corresponds to the ratio $\Delta h/h$. Therefore, taking account of (3), we have

$$\frac{\Delta h}{h} = \frac{c\Delta t}{\lambda} = \frac{2(n-1)l\Delta c - cl\Delta n}{\lambda c} \quad \text{or}$$

$$\Delta v \equiv \Delta c - \frac{c\Delta n}{2(n-1)} = \frac{c\lambda}{2(n-1)lh}\,\Delta h\,. \tag{4}$$

Substituting the known numerical parameters ($c = 3 \times 10^{10}$ cm s^{-1}, $\lambda = 6.33 \times 10^{-5}$ cm, $n = 1.53$, $l = 68$ cm, and $h = 0.7$ cm) we arrive at $\Delta v = 3.76 \times 10^4\,[s^{-1}]\,\Delta h\,[\text{cm}]$.

The shift of one of the interference minima from its mean position was determined for 12 orientations of the platform spaced by 30°. The deviation from zero of the parameter

sought was found to lie within the measurement error, which is 13 cm s^{-1} in units of Δv.

Considering the structure of Δv this means that either both constituents of Δv are rather small, namely, $|\Delta c| < 13$ cm s^{-1} and $|c\Delta n/2(n-1)| < 13$ cm s^{-1} (correspondingly, $|\Delta n| < 4.6 \times 10^{-10}$), or a relationship like $\Delta c = c\Delta n/2(n-1) + \varepsilon$ exists between them, where $|\varepsilon| < 13$ cm s^{-1}. Inserting the constraint $|\Delta n| < 5 \times 10^{-8}$ found in the earlier experiments into the last formula, we obtain $|\Delta c| < 14$ m s^{-1}, i.e. $|\Delta c|/c < 4.7 \times 10^{-8}$.

Thus, the experiments described demonstrate that the velocity of light in air, as well as the ratio of this velocity to that inside the glass (the refractive index), are independent of the direction of propagation to an accuracy not worse than 5×10^{-8}, and probably to 5×10^{-10}. Consequently, to the same accuracy laboratory space can be considered isotropic with respect to light propagation in substances of different density.

Of course, laboratory experiments cannot prove the answer about the isotropy of space far from the Earth. It would be therefore worthwhile carrying out similar experiments in this space.

References

1. Slyusarev G G, in *Fizicheskaya Éntsyklopediya* (Physical Encyclopedia) Vol. 3 (Moscow: Bol'shaya Sovetskaya Éntsiklopediya, 1992) p. 382
2. Ragul'skiĭ V V *Obrashchenie Volnovogo Fronta pri Vynuzhdennom Rasseyanii Sveta* (Optical Phase Conjugation by Stimulated Light Scattering) (Moscow: Nauka, 1990)
3. Arago F *Comptes Rendus* **36** 38 (1853)
4. Fizeau H *Comptes Rendus* **49** 717 (1859)
5. Brace D B *Philos. Mag.* Ser. 6 **10** 591 (1905)
6. Ragul'skiĭ V V *Pis'ma Zh. Eksp. Teor. Fiz.* **65** 497 (1997) [*JETP Lett.* **65** 517 (1997)]
7. Bonch-Bruevich A M, in *Fizicheskaya Éntsyklopediya* (Physical Encyclopedia) Vol. 4 (Moscow: Bol'shaya Rossiĭskaya Éntsiklopediya, 1994) p. 548
8. Froom K D, Essen L *The Velocity of Light and Radio Waves* (London: Butterworths, 1969) [Translated into Russian (Moscow: Mir, 1973) p. 12]
9. Illingworth K K *Phys. Rev.* **30** 692 (1927)
10. Marinov S *Indian J. Theor. Phys.* **39** 267 (1991)
11. Ragulsky V V *Phys. Lett. A* **235** 125 (1997)